Transient two-layer thin-film flow inside a channel

Kamran Alba,[1] Patrice Laure,[2] and Roger E. Khayat[1,*]

[1]*Department of Mechanical and Materials Engineering, University of Western Ontario, London, Ontario, Canada N6A 5B9*
[2]*Laboratoire J.-A. Dieudonné, CNRS UMR 6621, Université de Nice-Sophia Antipolis, Parc Valrose, F-06108 Nice Cedex 02, France*

The flow of two superimposed Newtonian layers in a channel is investigated numerically in this study. The two-layer film flows inside a long channel due to a pressure gradient. The scaled conservation equations for two-layer incompressible Newtonian film flow are first introduced. The weighted residual approach first proposed by Amaouche *et al.* [Phys. Fluids **19**, 084106 (2007)] is used for finding the suitable weight functions before depth averaging. Subsequently, a linear stability analysis of thin-film equations for two-layer Poiseuille flow is carried out. The formulas which give the asymptotic stability with respect to long-wave perturbations obtained with Navier-Stokes equations [J. Non-Newtonian Fluid Mech. **71**, 1 (1997)] are recovered with our averaging equations. In order to mimic the disturbance effect on the coextrusion flow, the steady flow, which is simply the uniform flow of two layers of fluid inside a channel, is then perturbed at inception. Following a finite difference based scheme, two types of boundary conditions are considered at the channel inception, namely a Dirac-type pulse and periodic forcing. The perturbation takes the form of a wave packet which may or may not be amplified as it moves downstream, depending on the values of the parameters involved in the problem. Furthermore, Gaster's relation is used to calculate the spatial growth rate of perturbation. The values obtained from this relation are in good quantitative agreement with those coming from the numerical simulations of thin-film equations. Then, our averaging equations also describe the nonlinear behavior of the interfacial instabilities occurring for the Poiseuille flow of two thin layers.

PACS number(s): 47.20.Ma

I. INTRODUCTION

The flow of two superimposed Newtonian layers is examined theoretically in this study. The fluid density is assumed to be uniform over the flow domain, but the viscosity in each layer can be different. Although the flow of a single-layer film inside a channel has been extensively investigated in the literature, less work has been devoted to multilayered films in the framework of thin-film approximation. One reason for the intense interest in thin-film flows is the wide variety of natural and industrial applications of such flows [1]. The multilayer configuration is mostly related to the industrial coextrusion process and coinjection molding [2]. The fluids used in coextrusion processes are mostly polymeric. Some important applications of coextrusion of the polymers can be found in markets related to alcohol-free beverages, fruit juices, functional drinks, noncarbonated water, food, etc. The standard is being set by smaller, high quality products for outdoor and fitness activities in user-friendly and secure plastic packages. In addition, plastic bottles and containers provide significant added values such as light weight, transportability, and recyclability. The beverage industry profits from multilayer packaging (coextrusion) through increased shelf life as well as taste and aroma protection, so that the products stay fresh without the use of preservatives.

In a coextrusion process, polymers are first melted in screw extruders separately and then flow simultaneously in the extrusion die. In some processing conditions wavy interfaces between the different polymer layers, due to the flow instability of the system in the die, are observed in the final product.

The thickness irregularity of each layer results in altered mechanical and optical properties. From the theoretical point of view, the occurrence of such interfacial instabilities has been analyzed by looking at the temporal stability of the two-layer plane Poiseuille flow. Earlier studies focused on Newtonian fluids both theoretically [3–9] and experimentally [10,11]. Joseph *et al.* [12] carried out a linear stability analysis for the flow of two immiscible fluids of different viscosities and equal density in a pipe. They showed that the volume ratio, related to the fluid thicknesses, is a crucial factor on the interface shape and stability. The Couette flow of two superposed viscous fluids in an infinite region was later studied by Hooper and Boyd [13]. They showed that the flow was always unstable due to short wavelength instabilities. Hooper [14] also showed that introducing a thin layer of viscous fluid next to the channel walls would have a destabilizing effect. Thereafter, the instability of two cocurrent superposed viscous fluids in a channel was examined by Hooper and Grimshaw [15]. They found that the interface may or may not be stable. In the latter case, the interface evolves to another steady state. Shankar and co-workers then looked at the stability analysis of a single and multilayer viscous flow past a deformable viscoelastic layer in two successive papers [16,17] to see how viscous layers adjacent to a wall can influence the stability of the lower viscoelastic layer.

The parameters controlling the stability of multilayer flow are the viscosity ratio, the thickness or flow rate ratio, and elasticity ratio in the case of the non-Newtonian fluids [18–23]. Thickness profiles and pressure drops across ducts and channels in two- and three-layer flows have been measured and estimated in early studies [24–26]. These studies were either motivated to reduce the pressure drop or to study the interface deformation in the form of encapsulation of the viscous fluid

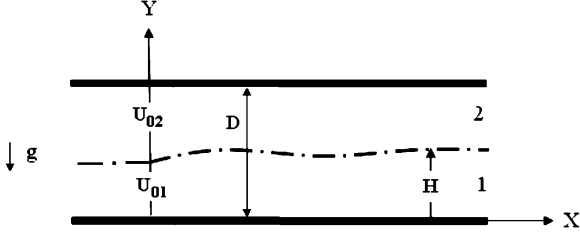*Corresponding author: rkhayat@uwo.ca

FIG. 1. Schematic illustration of two-layer thin-film flow in a channel. Dimensional notations are used.

by the fluid of low viscosity. The viscosity ratio is found to be the most important parameter as it affects the thickness and pressure drop.

Recently, Alba *et al.* [27] examined the steady flow of the two-layer thin Newtonian film theoretically. The film was assumed to emerge out of a channel and flow over a straight plate. Although the thin-film formulation reduces the pressure to its hydrostatic part, thus eliminating the momentum equation in the transverse direction from the problem, the dimension of the problem remains the same as in the original equation. At moderately high Reynolds number, inertia is better accounted for through the "boundary-layer" (BL) approximation, which includes the effect of transverse flow. The major difference between the original Navier-Stokes equations and the BL equations is the hydrostatic variation of pressure across the film depth. As a result, only the transverse momentum equation is eliminated, but the convective terms are retained in the remaining equations, and the number of boundary conditions is reduced. However, the solution of BL equations remains essentially as difficult to obtain as that of Navier-Stokes equations [28].

Film flow configuration is first introduced in Sec. II, and the scaled conservation equations for two-layer incompressible Newtonian film flow as well as the depth-averaged equations are discussed. In Sec. III, the stability of two-layer Poiseuille flow is investigated. Sec. IV examines the influence of boundary conditions at inception using a finite difference analysis. Two types of boundary conditions are considered, namely a Dirac-type pulse and periodic forcing. In Sec. V, Gaster's criterion [29] for computing the spatial growth rates is applied to the linear stability formulation. The predictions based on Gaster's criterion are then compared with those obtained through the numerical solution of the reduced model.

II. PROBLEM FORMULATION

In this section, the film flow configuration is introduced, and the scaled conservation equations for two-layer incompressible Newtonian film flow as well as the depth-averaged equations are discussed. The general form of the boundary and initial conditions is also outlined.

A. Thin-film equations

Consider the two-layer pressure-driven flow of incompressible Newtonian fluids moving inside a channel. Figure 1 displays schematically the flow configuration in the (X, Y)

plane. Layers 1 and 2 are taken to correspond to the lower and upper layer, respectively, with $H(X, T)$ being the height of the interface. The two layers have the same density, ρ, and different viscosities, μ_1 and μ_2. At inception ($X = 0$), the interface height is H_0 and layers 1 and 2 have mean flow velocities U_{01} and U_{02}, respectively. The mean flow velocity in the channel is denoted by U_0.

Reference scales are conveniently introduced in terms of the geometric and flow parameters of the mean flow and the lower layer. In this case, the channel thickness D is taken as the length scale in the depthwise direction, and U_0 is taken as the velocity scale streamwise. Consequently, the length scale in the streamwise direction is denoted by L, which is typically much larger than the channel thickness ($L \gg D$). The time scale is then defined as L/U_0. Assuming each layer to be thin, the following similarity parameters emerge in the problem, namely the Reynolds number Re, Froude number Fr, thickness-to-length ratio ε, the height ratio R_H, and viscosity ratio R_μ. More explicitly,

$$\mathrm{Re} = \frac{\rho U_0 D}{\mu_1}, \; \mathrm{Fr} = \frac{U_0^2}{Lg}, \; \varepsilon = \frac{D}{L}, \; R_H = \frac{D}{H_0}, \; R_\mu = \frac{\mu_2}{\mu_1},$$
(2.1)

where g is the gravitational acceleration acting in the negative Y direction. The velocity scale is taken to correspond to Poiseuille flow in the channel, which, in this case, is given by

$$U_0 = -\frac{dP}{dX}$$
$$\times \frac{H_0^2 \left[R_H^4 + (R_\mu - 1)\left(4R_H^3 - 6R_H^2 + 4R_H + R_\mu - 1\right)\right]}{12\mu_2(R_H + R_\mu - 1)R_H},$$

where $\frac{dP}{dX}$ is the steady-state constant pressure gradient. It is assumed that the temperature of the two fluid layers is kept constant inside the channel. In a real coextrusion process the cooling circuit will not be activated until the coextrusion flow reaches a steady regime inside the multimanifold die. Once a steady state is attained the extruded films are directed out of the die by a roll and cool down over a chilling path located after the roll. Therefore, during the coextrusion process the temperature of the melts does not vary much and since the viscous dissipation is also small (low shear rate in the system) we may neglect the energy equation in this context. In the industrial process of the coextrusion of polymers [for instance, polypropylene (PP) and high-density polyethylene (HDPE)], the Reynolds number is very small due to the high viscosities of polymers. Consequently, the shear rate will also be very small (often in the range of 1×10^{-5}/s to 0.1/s). The polypropylene and high-density polyethylene in this range of shear rate do not show a shear thinning behavior and act like a Newtonian fluid. Moreover the elasticity effects are also negligible in this case. Due to the presence of strong viscous forces in the coextrusion process, the flow can be assumed to be weakly inertial [Re = O(1)]. The conservation equations for thin-film flow are obtained in dimensionless form, with terms of $O(\varepsilon^2)$ and higher being excluded. In this case, the relevant equations

for the problem are

$$\frac{\partial u_1}{\partial x} + \frac{\partial v_1}{\partial y} = 0,$$

$$\frac{\partial u_1}{\partial t} + u_1 \frac{\partial u_1}{\partial x} + v_1 \frac{\partial u_1}{\partial y} = -\frac{1}{\varepsilon \text{Re}} \frac{\partial p_1}{\partial x} + \frac{1}{\varepsilon \text{Re}} \frac{\partial^2 u_1}{\partial y^2}, \quad (2.2)$$

$$\frac{\partial p_1}{\partial y} = -\frac{\text{Re} \varepsilon^2}{\text{Fr}},$$

for layer 1, and

$$\frac{\partial u_2}{\partial x} + \frac{\partial v_2}{\partial y} = 0,$$

$$\frac{\partial u_2}{\partial t} + u_2 \frac{\partial u_2}{\partial x} + v_2 \frac{\partial u_2}{\partial y} = -\frac{1}{\varepsilon \text{Re}} \frac{\partial p_2}{\partial x} + \frac{R_\mu}{\varepsilon \text{Re}} \frac{\partial^2 u_2}{\partial y^2}, \quad (2.3)$$

$$\frac{\partial p_2}{\partial y} = -\frac{\text{Re} \varepsilon^2}{\text{Fr}},$$

for layer 2. Here u, v, and p are the dimensionless velocity components in the x and y directions, and pressure, respectively, with subscripts corresponding to each layer. Note that εU_0 and $\frac{\mu_1 U_0}{\varepsilon D}$ are taken as depthwise velocity scale and pressure scale, respectively. Equations (2.2) and (2.3) can be solved subject to initial and boundary conditions at $t = 0$ and $x = 0$, respectively. Upon neglecting higher order terms in ε, the dynamic conditions at the interface reduce to

$$p_1 (x, y = h, t) = p_2 (x, y = h, t),$$
$$\frac{\partial u_1}{\partial y} (x, y = h, t) = R_\mu \frac{\partial u_2}{\partial y} (x, y = h, t), \quad (2.4)$$

where $h(x, t)$ represents the dimensionless height of the interface. The kinematic condition at the interface is given by

$$v_i (x, y = h, t) = \frac{\partial h}{\partial t} + \frac{\partial h}{\partial x} u_i (x, y = h, t), \quad (i = 1, 2). \quad (2.5)$$

No-slip and no-penetration conditions at the walls are assumed, so that

$$u_1 (x, y = 0, t) = u_2 (x, y = 1, t) = v_1 (x, y = 0, t)$$
$$= v_2 (x, y = 1, t) = 0. \quad (2.6)$$

The continuity of flow across the interface leads to

$$u_1 (x, y = h, t) = u_2 (x, y = h, t). \quad (2.7)$$

In this case, assuming no mass transfer across the interface leads to

$$v_1 (x, y = h, t) = v_2 (x, y = h, t). \quad (2.8)$$

At inception ($x = 0$), the height of the interface is assumed fixed, so that

$$h (x = 0, t) = \frac{1}{R_H}. \quad (2.9)$$

It is useful to introduce the parameter, R_Q, as the ratio of the steady flow rate of layer 2, Q_2^s, to the steady flow rate of layer 1, Q_1^s. In this case,

$$Q_1^s = \frac{1}{R_U R_H - R_U + 1}, \quad Q_2^s = \frac{R_U (R_H - 1)}{R_U R_H - R_U + 1}, \quad (2.10)$$

where R_U is the ratio of the mean velocity of layer 2 to the mean velocity of layer 1. Thus,

$$R_Q = \frac{Q_2^s}{Q_1^s} = R_U (R_H - 1),$$

$$R_U = \frac{(R_H - 1) \left[R_H^2 + 2 R_H (2 R_\mu - 1) - R_\mu + 1 \right]}{R_\mu \left(3 R_H^2 - 2 R_H + R_\mu - 1 \right)}. \quad (2.11)$$

B. Pressure elimination

Integrating the y-momentum equations in (2.2) and (2.3) simply gives the hydrostatic pressure distribution across the channel film, or

$$p_1 = -\frac{\text{Re} \varepsilon^2}{\text{Fr}} y + p_1 |_{y=0},$$

$$p_2 = -\frac{\text{Re} \varepsilon^2}{\text{Fr}} (y - h) + p_2 |_{y=h}. \quad (2.12)$$

The pressure in layer 1 is related to the wall shear stress, as seen upon evaluating the x-momentum equation at the wall to give

$$\left. \frac{\partial p_1}{\partial x} \right|_{y=0} = \left. \frac{\partial^2 u_1}{\partial y^2} \right|_{y=0}. \quad (2.13)$$

Using the dynamic condition at the interface, and noting from Eq. (2.12) that the streamwise pressure gradient is independent of y, one arrives at

$$\frac{\partial p_1}{\partial x} = \frac{\partial p_2}{\partial x} = \left. \frac{\partial^2 u_1}{\partial y^2} \right|_{y=0}. \quad (2.14)$$

Now, the x-momentum equations in (2.2) and (2.3) become

$$\varepsilon \text{Re} \left(\frac{\partial u_1}{\partial t} + u_1 \frac{\partial u_1}{\partial x} + v_1 \frac{\partial u_1}{\partial y} \right) = -\left. \frac{\partial^2 u_1}{\partial y^2} \right|_{y=0} + \frac{\partial^2 u_1}{\partial y^2}, \quad (2.15)$$

for layer 1, and

$$\varepsilon \text{Re} \left(\frac{\partial u_2}{\partial t} + u_2 \frac{\partial u_2}{\partial x} + v_2 \frac{\partial u_2}{\partial y} \right) = -\left. \frac{\partial^2 u_1}{\partial y^2} \right|_{y=0} + R_\mu \frac{\partial^2 u_2}{\partial y^2}, \quad (2.16)$$

for layer 2. Finally, conservation of mass dictates that

$$\int_0^h u_1 dy + \int_h^1 u_2 dy = 1 + f(t), \quad (2.17)$$

where $f(t)$ represents the time-dependent variation over the steady-state flow rate with a zero average value in time. This term is introduced to make direct numerical computations in a rigorous way in the last section. Indeed, the initial flow rate of the first layer will be perturbed, whereas its initial thickness is fixed. For linear analysis, both first layer flow rate and thickness are perturbed and then the total scaled flow rate is unitary.

A useful relation is obtained upon integrating the continuity equation in layer 1 and using the kinematic condition (2.5), namely

$$\frac{\partial h}{\partial t} + \frac{\partial q}{\partial x} = 0, \quad (2.18)$$

where $q = \int_0^h u_1 dy$ is the flow rate in layer 1.

III. REDUCED PROBLEM

The problem is now reduced to a two-equation model by using the weighted residual method similarly to Quil and Manneville [30] for falling thin film of Newtonian fluid and Amaouche *et al.* [31]. The method consists of projecting the velocity field in each layer onto a basis of functions which satisfies the no-slip condition at the walls.

A. Velocity field expansion

The streamwise velocity components are expanded in powers of ε as

$$u_i(x,y,t) = u_i^{(0)} + \varepsilon u_i^{(1)} + O(\varepsilon^2), \, i = 1,2. \quad (3.1)$$

The transverse velocity component in each layer is then determined upon using Eq. (3.1) and integrating the continuity equation, to give

$$v_1(x,y,t) = -\int_0^y \frac{\partial u_1}{\partial x} dy = -\int_0^y \frac{\partial u_1^{(0)}}{\partial x} dy - \varepsilon \int_0^y \frac{\partial u_1^{(1)}}{\partial x} dy + O(\varepsilon^2), \quad (3.2a)$$

$$v_2(x,y,t) = v_1(x, y = h, t) - \int_h^y \frac{\partial u_2}{\partial x} dy = v_1(x, y = h, t) - \int_h^y \frac{\partial u_2^{(0)}}{\partial x} dy - \varepsilon \int_h^y \frac{\partial u_2^{(1)}}{\partial x} dy + O(\varepsilon^2). \quad (3.2b)$$

Substituting expansions (3.1) back into the x-momentum equations (2.15) and (2.16) indicates that the leading order solutions, $u_1^{(0)}$ and $u_2^{(0)}$, are maximum of degree 2 in y, or

$$u_i^{(0)}(x,y,t) = A_i(x,t) y^2 + B_i(x,t) y + C_i(x,t), \, i = 1,2. \quad (3.3)$$

The coefficients are yet to be determined. By suitable choice of weight functions we do not need to calculate $u_1^{(1)}$ and $u_2^{(1)}$ (see later). However, additional assumptions are made on the first-order corrections $u_i^{(1)}$,

$$\int_0^h u_1^{(1)} dy = 0 \text{ and } \int_h^1 u_2^{(1)} dy = 0, \quad (3.4)$$

in order to simplify the choice of weight functions. These assumptions mean that the flow rates in each layer are accurately approximated by the zero order approximation of expansion (3.1). This assumption has an influence only on the terms $u_1^{(1)}$ and $u_2^{(1)}$, which are not important for the first-order effect described by our thin limit equations. Moreover, these assumptions simplify the approach of Amouache [31] which needs the computations of 14 additional unknowns. It is worth noting that by setting conditions (3.4), we are restricting the solutions to a subset of all the possible ones. However, these solutions matter when one wants to consider first-order velocity terms too (second-order accurate method). In this study, we are interested in first-order accuracy. Therefore, the assumptions made on the integrals are justifiable.

It is not difficult to show from conditions (2.4), (2.6), and (2.7), and Eq. (2.17), that

$$A_1 = -\frac{3}{2h^3} \frac{[(R_\mu - 1)q + 3R_\mu(1+f)]h^2 + [2(1-2R_\mu)h - 1]q}{(R_\mu - 1)h^2 + (2 - R_\mu)h - 1},$$

$$B_1 = \frac{3}{h^2} \frac{[R_\mu(1+f) + (R_\mu - 1)q]h^2 + [2h(1-R_\mu) - 1]q}{(R_\mu - 1)h^2 + (2 - R_\mu)h - 1},$$

$$C_1 = 0,$$

$$A_2 = -\frac{3}{2h} \frac{[(4 - R_\mu)(1+f) + (R_\mu - 1)q]h^2 - 4(1+f)h + (3-2h)q}{(R_\mu - 1)h^4 + (4 - 3R_\mu)h^3 + 3(R_\mu - 2)h^2 + (4 - R_\mu)h - 1}, \quad (3.5)$$

$$B_2 = \frac{3}{h} \frac{[(1+f)(2 - R_\mu) + (R_\mu - 1)q]h^3 - 2(1+f)h + (2-h)q}{(R_\mu - 1)h^4 + (4 - 3R_\mu)h^3 + 3(R_\mu - 2)h^2 + (4 - R_\mu)h - 1},$$

$$C_2 = -\frac{3}{2h} \frac{2[(2 - R_\mu)(1+f) + (R_\mu - 1)q]h^3 + [(R_\mu - 4)(1+f) + (1 - R_\mu)q]h^2 + q}{(R_\mu - 1)h^4 + (4 - 3R_\mu)h^3 + 3(R_\mu - 2)h^2 + (4 - R_\mu)h - 1}.$$

The depthwise velocity component to leading order is then obtained from Eqs. (3.2) and (3.3), to become

$$v_1^{(0)}(x,y,t) = -\frac{\partial A_1}{\partial x} \frac{y^3}{3} - \frac{\partial B_1}{\partial x} \frac{y^2}{2}, \quad (3.6a)$$

$$v_2^{(0)}(x,y,t) = v_1^{(0)}(x, y = h, t) - \frac{\partial A_2}{\partial x} \left(\frac{y^3 - h}{3}\right) - \frac{\partial B_2}{\partial x} \left(\frac{y^2 - h}{2}\right) - \frac{\partial C_2}{\partial x}(y - h). \quad (3.6b)$$

B. Weighted residual approach

Now that the dependency of the leading order streamwise velocity components on y is established, the x-momentum equations (2.15) and (2.16) can now be integrated with respect to y. Significant simplification is made if, before the integration, we multiply the x-momentum equations by some suitable weight functions, $g_1(x,y,t)$ and $g_2(x,y,t)$, say, which will be defined in such a way that the averaged equations are no longer dependent on the first-order terms in the velocity field expansion. Projecting the x-momentum equations (2.15) and (2.16) with respect to y and summing them results in

$$\int_0^h \left[\varepsilon \mathrm{Re} \left(\frac{\partial u_1^{(0)}}{\partial t} + u_1^{(0)} \frac{\partial u_1^{(0)}}{\partial x} + v_1^{(0)} \frac{\partial u_1^{(0)}}{\partial y} \right) + \frac{\partial^2 u_1^{(0)}}{\partial y^2} \bigg|_{y=0} + \varepsilon \frac{\partial^2 u_1^{(1)}}{\partial y^2} \bigg|_{y=0} - \frac{\partial^2 u_1^{(0)}}{\partial y^2} - \varepsilon \frac{\partial^2 u_1^{(1)}}{\partial y^2} \right] g_1 dy$$

$$+ \int_h^1 \left[\varepsilon \mathrm{Re} \left(\frac{\partial u_2^{(0)}}{\partial t} + u_2^{(0)} \frac{\partial u_2^{(0)}}{\partial x} + v_2^{(0)} \frac{\partial u_2^{(0)}}{\partial y} \right) + \frac{\partial^2 u_1^{(0)}}{\partial y^2} \bigg|_{y=0} + \varepsilon \frac{\partial^2 u_1^{(1)}}{\partial y^2} \bigg|_{y=0} - R_\mu \frac{\partial^2 u_2^{(0)}}{\partial y^2} - \varepsilon R_\mu \frac{\partial^2 u_2^{(1)}}{\partial y^2} \right] g_2 dy. \quad (3.7)$$

Thus, to first order, the correction $u_i^{(1)}$ of the leading velocity field would appear only through the diffusive terms

$$\left(\int_0^h g_1 dy + \int_h^1 g_2 dy \right) \frac{\partial^2 u_1^{(1)}}{\partial y^2} \bigg|_{y=0}$$

and

$$\int_0^h \frac{\partial^2 u_1^{(1)}}{\partial y^2} g_1 dy + R_\mu \int_h^1 \frac{\partial^2 u_2^{(1)}}{\partial y^2} g_2 dy.$$

One can then eliminate the explicit effects of this correction from Eq. (3.7) with appropriate choice of the weight functions g_i. Hence, a fully consistent first-order model would include only the leading-order velocity field. In the following, the contribution of terms of order ε^2 will be neglected, which renders the model fully consistent up to first order with respect to ε. Moreover, with a suitable choice of the weight function g_i one can eliminate the first-order contribution of the correction altogether . Clearly, in this case, one sets

$$\int_0^h g_1 dy + \int_h^1 g_2 dy = 0. \quad (3.8)$$

In this case, Eq. (3.7) becomes

$$\int_0^h \left[\varepsilon \mathrm{Re} \left(\frac{\partial u_1^{(0)}}{\partial t} + u_1^{(0)} \frac{\partial u_1^{(0)}}{\partial x} + v_1^{(0)} \frac{\partial u_1^{(0)}}{\partial y} \right) - \frac{\partial^2 u_1^{(0)}}{\partial y^2} - \varepsilon \frac{\partial^2 u_1^{(1)}}{\partial y^2} \right] g_1 dy$$

$$+ \int_h^1 \left[\varepsilon \mathrm{Re} \left(\frac{\partial u_2^{(0)}}{\partial t} + u_2^{(0)} \frac{\partial u_2^{(0)}}{\partial x} + v_2^{(0)} \frac{\partial u_2^{(0)}}{\partial y} \right) - R_\mu \frac{\partial^2 u_2^{(0)}}{\partial y^2} - \varepsilon R_\mu \frac{\partial^2 u_2^{(1)}}{\partial y^2} \right] g_2 dy = 0. \quad (3.9)$$

Using double integration by parts and with the aide of the no-slip condition equation (2.6), the first-order diffusive terms are rewritten in the form

$$\int_0^h \frac{\partial^2 u_1^{(1)}}{\partial y^2} g_1 dy + R_\mu \int_h^1 \frac{\partial^2 u_2^{(1)}}{\partial y^2} g_2 dy = g_1 (x,h,t) \frac{\partial u_1^{(1)}}{\partial y} \bigg|_{y=h} - g_1 (x,0,t) \frac{\partial u_1^{(1)}}{\partial y} \bigg|_{y=0} + R_\mu g_2 (x,1,t) \frac{\partial u_2^{(1)}}{\partial y} \bigg|_{y=1}$$

$$- R_\mu g_2 (x,h,t) \frac{\partial u_2^{(1)}}{\partial y} \bigg|_{y=h} - u_1^{(1)} (h) \frac{\partial g_1}{\partial y} \bigg|_{y=h} + R_\mu u_2^{(1)} (h) \frac{\partial g_2}{\partial y} \bigg|_{y=h} + \int_0^h u_1^{(1)} \frac{\partial^2 g_1}{\partial y^2} dy + R_\mu \int_h^1 u_2^{(1)} \frac{\partial^2 g_2}{\partial y^2} dy. \quad (3.10)$$

Thus, the elimination of the explicit contribution of the first-order correction is possible upon first recalling the dynamic condition (2.4) and velocity continuity (2.7) across the interface. In this case, relation (3.10) becomes

$$\int_0^h \frac{\partial^2 u_1^{(1)}}{\partial y^2} g_1 dy + R_\mu \int_h^1 \frac{\partial^2 u_2^{(1)}}{\partial y^2} g_2 dy = -g_1 (x,0,t) \frac{\partial u_1^{(1)}}{\partial y} \bigg|_{y=0} + R_\mu g_2 (x,1,t) \frac{\partial u_2^{(1)}}{\partial y} \bigg|_{y=1} + [g_1 (x,h,t) - g_2 (x,h,t)] \frac{\partial u_1^{(1)}}{\partial y} \bigg|_{y=h}$$

$$- u_1^{(1)} (h) \left(\frac{\partial g_1}{\partial y} \bigg|_{y=h} - R_\mu \frac{\partial g_2}{\partial y} \bigg|_{y=h} \right) + \int_0^h u_1^{(1)} \frac{\partial^2 g_1}{\partial y^2} dy + R_\mu \int_h^1 u_2^{(1)} \frac{\partial^2 g_2}{\partial y^2} dy. \quad (3.11)$$

Clearly, the following conditions can now be set to eliminate the dependency of the solution on $u_1^{(1)}$ and $u_2^{(1)}$, namely

$$\frac{\partial g_1}{\partial y} \bigg|_{y=h} - R_\mu \frac{\partial g_2}{\partial y} \bigg|_{y=h} = 0,$$

$$g_1 (x,h,t) = g_2 (x,h,t),$$

$$g_1 (x,0,t) = g_2 (x,1,t) = 0. \quad (3.12)$$

If g_i are chosen as polynomials in y, then they must be of at least second degree. Otherwise, conditions (3.12) lead to $g_i = 0$ for any y. In this case, g_i are given as

$$g_i(x,y,t) = D_i(x,t)y^2 + E_i(x,t)y + F_i(x,t), \quad (3.13)$$

where D_i, E_i, and F_i are unknown functions of x and t. Conditions (3.8) and (3.12) provide five of the six equations to determine the coefficients D_i, E_i, and F_i. In this case,

$$g_1 = [y^2 - 2\frac{(R_\mu - 1)h^2 + 2(1 - R_\mu)h - 1}{(R_\mu - 1)h^2 + 2(1 - 2R_\mu)h - 1}hy]D_1,$$

$$g_2 = \frac{[(R_\mu - 1)h^2 - 2h + 3]y^2 - 2[(R_\mu - 1)h^3 - h + 2]y + 2(R_\mu - 1)h^3 - (R_\mu - 1)h^2 + 1}{(h-1)^2[(R_\mu - 1)h^2 + 2(1 - 2R_\mu)h - 1]}h^2D_1. \quad (3.14)$$

The value of D_1 will turn out to be immaterial. Indeed, Eq. (3.11) reduces to an expression containing only the perturbation flow rates, namely,

$$\int_0^h \frac{\partial^2 u_1^{(1)}}{\partial y^2}g_1 dy + R_\mu \int_h^1 \frac{\partial^2 u_2^{(1)}}{\partial y^2}g_2 dy$$

$$= D_1 \int_0^h u_1^{(1)}dy + R_\mu D_2 \int_h^1 u_2^{(1)}dy, \quad (3.15)$$

which is null thanks to assumptions (3.4). Finally, Eq. (3.8) reduces to

$$\int_0^h \left[\varepsilon \text{Re}\left(\frac{\partial u_1^{(0)}}{\partial t} + u_1^{(0)}\frac{\partial u_1^{(0)}}{\partial x} + v_1^{(0)}\frac{\partial u_1^{(0)}}{\partial y}\right) - \frac{\partial^2 u_1^{(0)}}{\partial y^2}\right]g_1 dy$$

$$+ \int_h^1 \left[\varepsilon \text{Re}\left(\frac{\partial u_2^{(0)}}{\partial t} + u_2^{(0)}\frac{\partial u_2^{(0)}}{\partial x} + v_2^{(0)}\frac{\partial u_2^{(0)}}{\partial y}\right)\right.$$

$$\left. - R_\mu\frac{\partial^2 u_2^{(0)}}{\partial y^2}\right]g_2 dy = 0. \quad (3.16)$$

Substituting Eqs. (3.3), (3.5), and (3.14) into Eq. (3.16) along with the use of kinematic condition (2.18) results in the following system of equations:

$$\frac{\partial h}{\partial t} + \frac{\partial q}{\partial x} = 0,$$

$$R_1\frac{\partial h}{\partial t} + R_2\frac{\partial h}{\partial x} + R_3\frac{\partial q}{\partial t} + R_4\frac{\partial q}{\partial x} + R_5 = 0, \quad (3.17)$$

where the superscript (0) is dropped for convenience. Here the coefficients $R_1, R_2,..., R_5$ are explicit functions of q, h, and f and are given in Appendix A. Please note that the equations are rescaled so that ε no longer appears in Eq. (3.17). In other words, the independent variables of the problem, x and t, have been replaced by εx and εt, respectively. It is worth mentioning that the accuracy of Shkadov's approach [32] is of order 1, whereas the current method results in an $O(\varepsilon)$ accuracy. The reason is that the weight functions are simply unity in Shkadov's approach. Amaouche *et al.* [31] also showed that the depth-averaging method with unity weight functions cannot predict the onset of linear instability correctly.

IV. LINEAR STABILITY ANALYSIS

The stability of steady two-layer Poiseuille flow is investigated in this section using the system of equations (3.17). The steady state is obtained upon setting the time derivatives to zero, leading to a nonlinear system of equations for q and h, which may have multiple solutions. The simplest steady flow corresponds to the Poiseuille profile in each layer and a flat interface. The stability of this two-layer Poiseuille flow will be analyzed in this work. The steady state is governed by

$$h^s = \frac{1}{R_H}, \quad q^s = \frac{1}{R_U R_H - R_U + 1}, \quad (4.1)$$

as $q^s = Q_1^s$. Imposing a small perturbation on the steady state leads to

$$h = h^s + \tilde{h}, \quad q = q^s + \tilde{q}. \quad (4.2)$$

Substituting Eq. (4.2) into Eq. (3.17) leads to the following linearized system of equations:

$$\frac{\partial \tilde{h}}{\partial t} + \frac{\partial \tilde{q}}{\partial x} = 0,$$

$$R_1^s\frac{\partial \tilde{h}}{\partial t} + R_2^s\frac{\partial \tilde{h}}{\partial x} + R_3^s\frac{\partial \tilde{q}}{\partial t} + R_4^s\frac{\partial \tilde{q}}{\partial x} + \frac{\partial R_5}{\partial h}\bigg|^s \tilde{h} + \frac{\partial R_5}{\partial q}\bigg|^s \tilde{q} = 0, \quad (4.3)$$

governing the perturbations. The coefficients $R_1^s, R_2^s,..., R_5^s$ are the same as $R_1, R_2,..., R_5$ given in Appendix A except in this case, q and h are replaced by their corresponding steady-state values from Eq. (4.1) and $f(t)$ has been set equal to zero. The perturbations are assumed to be periodic in x, so that

$$\tilde{h} = \bar{h}e^{i\alpha x + \sigma t}, \quad \tilde{q} = \bar{q}e^{i\alpha x + \sigma t}, \quad (4.4)$$

where $\bar{h}$ and $\bar{q}$ are constants. Substituting Eq. (4.4) into Eq. (4.3) leads to a dispersion relation which is quadratic in σ:

$$D(\sigma, \alpha, R_H, \text{Re}, R_\mu)$$

$$= \begin{vmatrix} \sigma & i\alpha \\ R_1^s\sigma + R_2^s i\alpha + \partial_h R_5^s & R_3^s\sigma + R_4^s i\alpha + \partial_q R_5^s \end{vmatrix} = 0. \quad (4.5)$$

If the real part of any of the σ roots is positive, the flow is linearly unstable. Yih [3] pointed out that the interfacial mode is neutrally stable when the fluids have the same viscosity $R_\mu = 1$. In a later study, Yiantsios and Higgins found that the interfacial mode is also neutrally stable when $R_\mu = (R_H - 1)^2$ [6]. These results are also found with dispersion relation (4.5) as there are eigenvalues with zero real part,

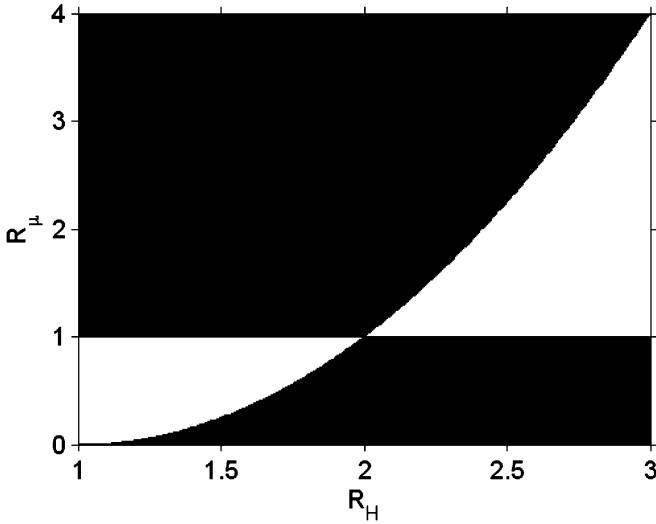$$\sigma = -6i\alpha\frac{R_H - 1}{R_H^2} \quad \text{and} \quad \sigma = -\frac{3}{2}i\alpha, \quad (4.6)$$

FIG. 2. Stability diagram in the (R_H, R_μ) plane in the long wavelength limit ($\alpha \to 0$). The black and white regions show that the Poiseuille profile is unstable or stable, respectively.

for $R_\mu = 1$ and $R_\mu = (R_H - 1)^2$, respectively (the other eigenvalue has a negative real part). Moreover, the long-wave analysis ($\alpha \to 0$) can be classically made by expanding the eigenvalue around $\alpha = 0$,

$$\sigma = -i\alpha\left(c_0 + \alpha c_1 + \cdots\right), \qquad (4.7)$$

This expansion is put in the relation (4.5) and the cancellation of the first terms of the polynomial in α gives equations allowing the computation of the two coefficients. It is found that c_0 is real and c_1 purely imaginary:

$$c_1 = i\mathrm{Re}(R_\mu - 1)[R_\mu - (R_H - 1)^2]F(R_H, R_\mu). \quad (4.8)$$

The analytical expressions of c_0 and c_1 are given in Appendix B. We point out that the expressions given in [22] which correspond to the long-wave analysis of the Navier-Stokes equations are recovered. Then, Fig. 2, which shows the stability diagram in the (R_H, R_μ) plane, is in complete agreement with the results of Yiantsios and Higgins [6] in the long-wave-length limit. The black and white regions show that the Poiseuille profile is unstable and stable, respectively. It is verified that the two-layer Poiseuille flow is stable when the less viscous layer is sufficiently thin (thin lubrication layer effect). The neutral curves in Fig. 2 correspond to the lines $R_\mu = 1$ and $R_\mu = (R_H - 1)^2$ which remain independent of the Reynolds number. The latter curve represents the case when the slope of the base velocity profile, and hence the vorticity distribution, is continuous at the interface.

Vempati *et al.* [33] recently carried out a linear stability analysis for two-layer flow in an inclined channel. They found out that the critical value of the flow rate (or equivalently the Reynolds number) for the onset of instability determined from the measurements is larger than that predicted by linear stability analysis at all tilt angles and interface heights. The reason for this discrepancy is the lack of accuracy of the visualization technique used for experimental measurement, preventing the visualization of the small disturbance waves. In addition, the
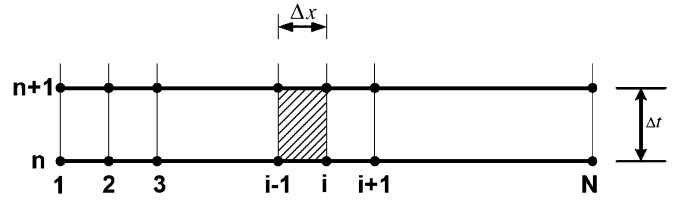

FIG. 3. Mesh of the solution procedure.

test sections used in the experiment were not chosen long enough to see the unstable interfacial disturbances.

V. NONLINEAR TRANSIENT RESPONSE

The formulation in the previous section is now used to investigate transient nonlinear two-layer film flow. A brief outline of the solution procedure is given first. The steady flow, which is simply the uniform flow of two layers of fluid inside the channel, is perturbed by imposing a time-dependent forcing on the lower-layer flow rate at inception ($x = 0$). The response to two types of forcing at inception is examined, namely an initial pulse of the Dirac type, and a time-periodic forcing. These boundary conditions are taken to investigate the effect of pump perturbations on the quality of coextruded layers. Finally, some connection with coextrusion will be made.

A. Solution method

The system of nonlinear equations (3.17) is discretized in the x-t domain. Keller's box method [34] is used to solve the discretized equations. Figure 3 shows the mesh used in this discretization. The step size and time step used along the x axis and time are $\Delta x = 0.1$ and $\Delta t = 0.01$, respectively. These values are found to lead to reasonable accuracy, stability, and convergence rate, and are fixed in all the numerical calculations presented in this study. The derivatives in Eq. (3.17) are as follows:

$$
\begin{aligned}
\frac{\partial h}{\partial t} &= \frac{\left(h_i^{n+1} + h_{i-1}^{n+1} - h_i^n - h_{i-1}^n\right)}{2\Delta t}, \\
\frac{\partial q}{\partial t} &= \frac{\left(q_i^{n+1} + q_{i-1}^{n+1} - q_i^n - q_{i-1}^n\right)}{2\Delta t}, \\
\frac{\partial h}{\partial x} &= \frac{\left(h_i^{n+1} + h_i^n - h_{i-1}^{n+1} - h_{i-1}^n\right)}{2\Delta x}, \\
\frac{\partial q}{\partial x} &= \frac{\left(q_i^{n+1} + q_i^n - q_{i-1}^{n+1} - q_{i-1}^n\right)}{2\Delta x}.
\end{aligned}
\qquad (5.1)
$$

The time-dependent boundary conditions at inception will be specified later in Secs. V B and V C. The steady flow, which is simply the uniform flow of two layers of fluid inside the channel, is taken as initial condition at $t = 0$ [see relations (4.1)]. Given the initial and boundary conditions, the values of h and q at nodes (i, n), (i, n) $(i, n + 1)$ in Fig. 3 are then known. Moreover, it can be seen from Eq. (5.1) that the time derivatives are approximated in an implicit manner not to impose any restrictions on the maximum allowable time step and also to ensure numerical stability. The coefficients $R_1, R_2, ..., R_5$ in Eq. (3.17) are nonlinear functions of h and q

(see Appendix A), which are taken as average values over the cell shown in Fig. 3, or

$$h = \frac{h_{i-1}^{n+1} + h_i^{n+1} + h_{i-1}^n + h_i^n}{4},$$

$$q = \frac{q_{i-1}^{n+1} + q_i^{n+1} + q_{i-1}^n + q_i^n}{4}. \tag{5.2}$$

The kinematic condition in Eq. (3.17) is a linear partial differential equation. Using the first equations in systems (3.17) and (5.1), it is not difficult to relate h_i^{n+1} to q_i^{n+1}. The nonlinear depth-averaged momentum equation in Eq. (3.17) can now be used to solve for q_i^{n+1}. The Newton-Raphson root-finding method is then used to find q_i^{n+1}, the lower-layer flow rate at the new time step.

B. Dirac-type pulse forcing

In this section, it is assumed that a sudden pulse is imposed for the flow rate of the lower layer, which has the following form:

$$q(x = 0, t) = q^s + 0.1 q^s \delta(t), \tag{5.3}$$

where $\delta(t)$ is the Dirac delta function. Figure 4 displays the profiles of the interface evolution, $h–h^s$ (h^s is the steady interface height), for two different Re values at $x = 1$. It can be seen that the modified Reynolds number has a destabilizing effect on the flow as reflected by the increase in the modulation amplitude. The perturbation takes the form of a wave packet. In fact, the interface oscillates and then decays to its steady value, over a longer time for Re = 10 than for Re = 1. Similar behavior was previously observed by Valette *et al.* [35] for both Newtonian and viscoelastic fluids using the finite element method and the Navier-Stokes equations.

The evolution of the interface at two different locations (x = 1 and 2) is illustrated in Fig. 5 for a Dirac-type pulse for $R_\mu = 0.1$, $R_Q = 2.3$, and Re = 10. Note that for this set of parameters, the thickness ratio is $R_H = 2$ upon using Eq. (2.11). As is evident from this figure, the maximum modulation amplitude increases further downstream (such systems are mainly noise amplifier). The perturbation is convected along the x axis and remains localized. Therefore, it is concluded that the interfacial instability for the moderate modified Reynolds number is of the convective type [36]. In general, if small localized disturbances grow in time at the location of excitation, the flow is termed as absolutely linearly unstable, and if they propagate away from their original location without changing the basic state flow, the flow is convectively unstable. In the two-layer channel flow, the perturbation takes the form of a wave packet which may or may not be amplified as it moves downstream. The spatial evolution of the unsteady flow is in large part determined by the character of the excitation, e.g., amplitude, frequency, etc. It is worth noting that Laure and Fortin [37] have obtained the same qualitative behavior with the Navier-Stokes equations for a channel with finite length using the same viscosity ratio ($R_\mu = 0.1$) but larger flow rate ratio ($R_Q = 11.5$).

Figure 6 shows the interface evolution at $x = 1$ and 2 for $R_\mu = 0.1$, $R_Q = 0.11$, and Re = 10. The corresponding thickness ratio value in this case is $R_H = 1.15$. Upon
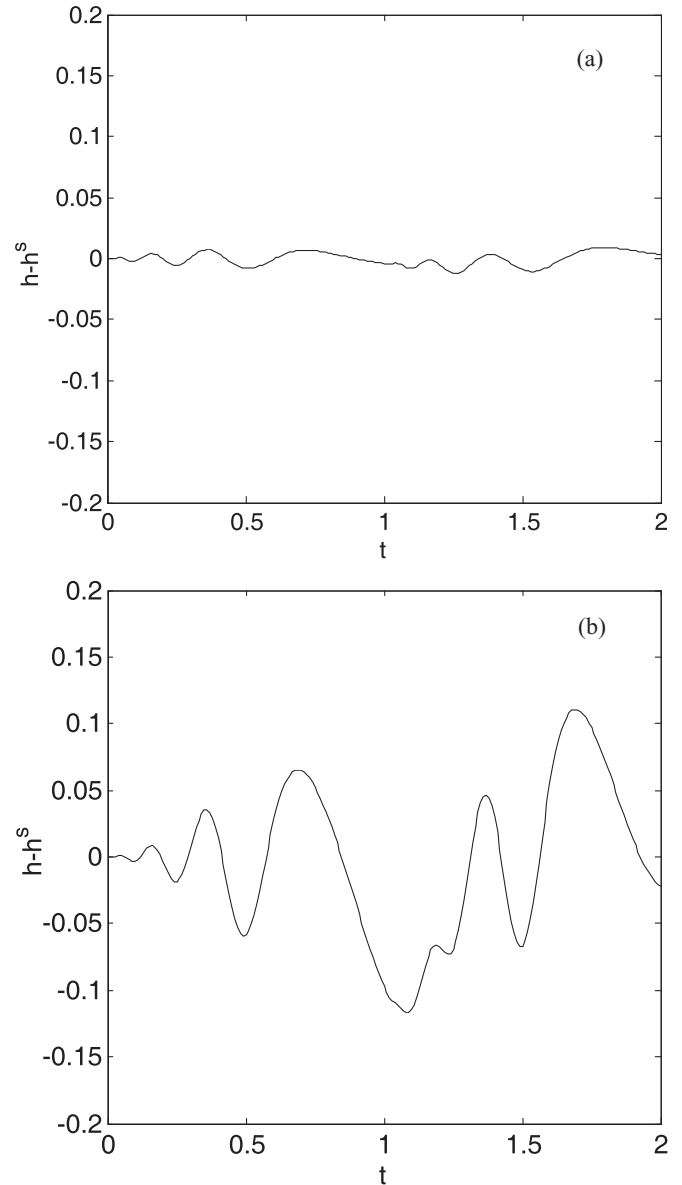

FIG. 4. The interface evolution at $x = 1$ with time for $R_\mu = 0.1$ and $R_Q = 11.5$ for (a) Re = 1 and (b) Re = 10. The forcing is a Dirac-type pulse.

comparing Figs. 5 and 6, it can be seen that the modulation amplitude is damped further downstream. Given the same set of parameters, the behavior shown in Fig. 6 has also been reported in [37] for a channel of finite length using a Galerkin finite element method for the direct numerical computations of Navier-Stokes equations.

C. Time-periodic forcing

This type of forcing can be related to the extruder rotary motion, and it is probable to have a periodic perturbation imposed on the layer flow rates. The periodic excitation is a conventional way of assessing the multilayer stability. Wilson and Khomami [38] perturbed the two-layer flow by regulating a pressure pulse periodically, which finally results in the change in the flow rate. In this section, the effect of a time-periodic boundary condition on the coextrusion flow will be examined.
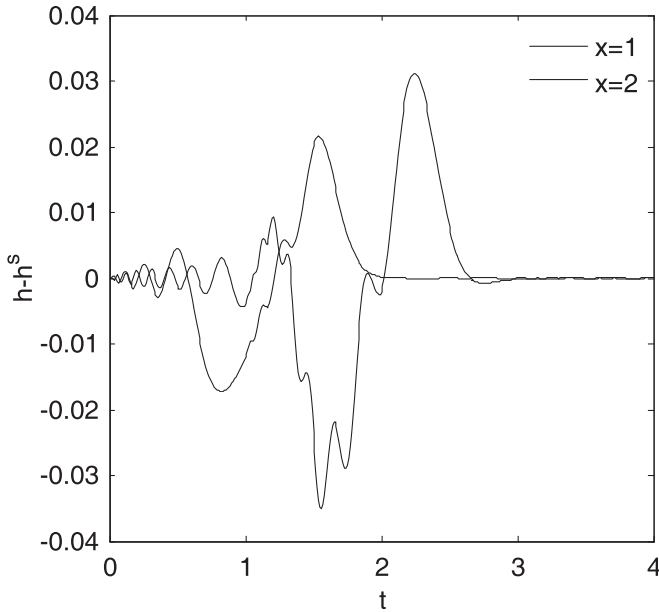
FIG. 5. The interface evolution with time at two different locations for $R_\mu = 0.1$, Re $= 10$ and $R_Q = 2.3$ ($R_H = 2$). The forcing is a Dirac-type pulse.

The lower-layer flow rate at inception is now perturbed in the following form:

$$q\,(x = 0,t) = q^s + 0.1q^s \sin\,(2\pi\nu t)\,, \qquad (5.4)$$

where ν is the forcing frequency. The interface height evolution at two different locations ($x = 1$ and 2) is illustrated in Fig. 7 for $R_Q = 2.3$. These two points are, respectively, located near and away from the inception. The other parameters are $R_\mu = 0.1$, Re $= 10$, and $\nu = 1/2$. Further downstream, the maximum
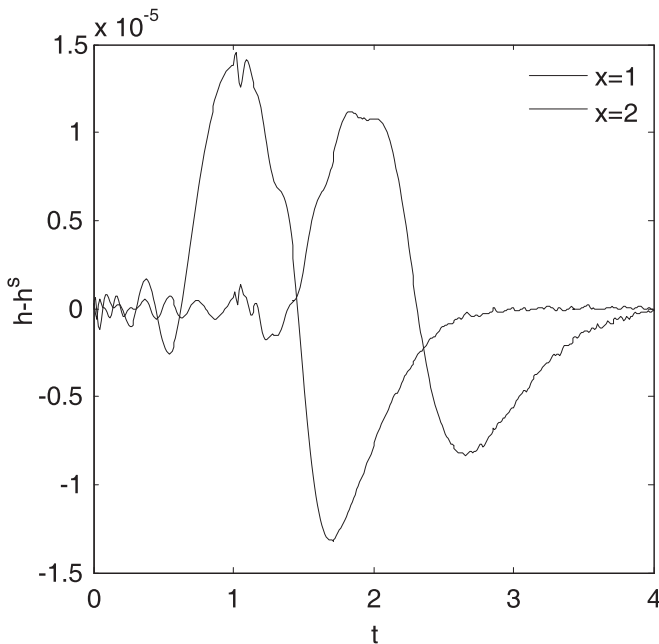

FIG. 6. The interface evolution with time at two different locations for $R_\mu = 0.1$ and Re $= 10$ and $R_Q = 0.11$ ($R_H = 1.15$). The forcing is of the Dirac-type pulse.
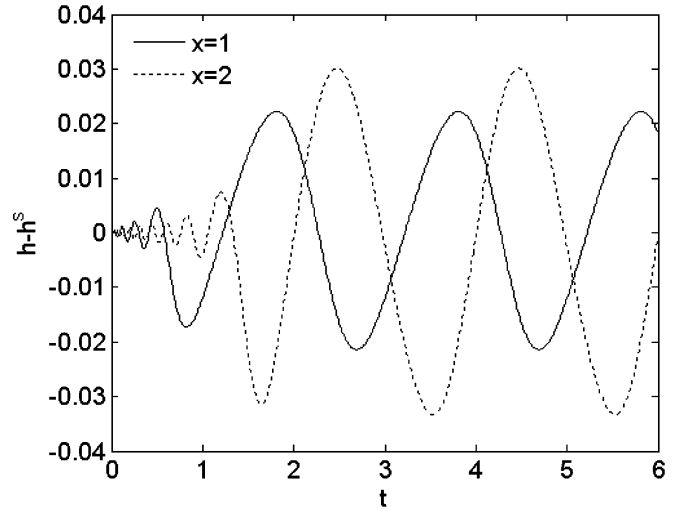

FIG. 7. The interface evolution with time at two different locations for $R_\mu = 0.1$ and Re $= 10$ for $R_Q = 2.3$ ($R_H = 2$). The forcing frequency is $\nu = \frac{1}{2}$.

modulation amplitude is amplified. There is always a time delay for a point at a further location affected by the flow rate change at inception (see Fig. 4). This time delay is in general a function of the flow characteristics such as R_μ, R_Q, and, more importantly, Re. In the case of the time-periodic forcing, similarly to the Dirac-type pulse case, the amplifying behavior of the flow field becomes more evident by further increasing the R_Q value [37].

Finally, Fig. 8 displays the interface evolution at $x = 1$ and 2 for fairly low value of flow rate ratio ($R_Q = 0.11$). The other parameters are kept the same as in Fig. 7. Upon comparing Figs. 7 and 8, it is observed that, similarly to the Dirac-type pulse case, the modulation amplitudes for these values of R_μ and R_Q will be damped further downstream for time-periodic forcing. The behavior shown in Fig. 8 for periodic forcing is confirmed via direct simulation of the Navier-Stokes equations [37].

D. Connection with coextrusion

Suppose that the upper layer is 2.5 mm thick and contains polypropylene (PP) melt and the lower layer is also 2.5 mm thick but contains high-density polyethylene (HDPE) melt. The thickness ratio at inception is then obtained as $R_H = 2$. The channel length is assumed to be large enough compared to its thickness. The value of the thickness-to-length ratio, ε, will be a small value and the thin-film approach remains valid. The melt flow rate in this coextrusion process is often very low and at 200 °C may be around 30 g/min. Using this flow rate, it is not difficult to show that the mean velocity inside a 5-mm-wide channel is $U = 1.05 \times 10^{-4}$ m/s and the maximum shear rate across the channel becomes 0.04 m/s. In this range of shear rate, the polymers can be modeled as Newtonian fluid. The viscosities of polypropylene and high-density polyethylene at 200 °C are approximately equal to 2×10^3 and 2×10^4 Pa s, respectively, and their density is taken to be $\sim$950 kg/m^3. In this case, the Reynolds number is of order 10^{-7} and the viscosity ratio $R_\mu = 0.1$. The current formulation suggests that if the speed of screw extruder of high-density polyethylene
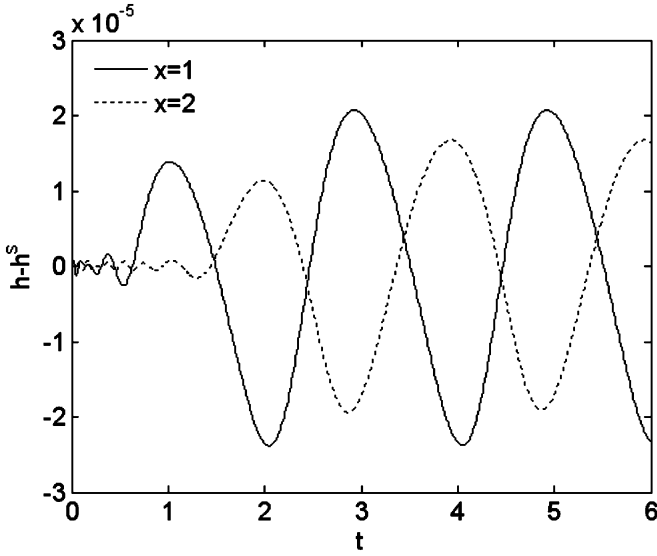
FIG. 8. The interface evolution with time at two different locations for $R_\mu = 0.1$ and Re $= 10$ for $R_Q = 0.11$ ($R_H = 1.15$). The forcing frequency is $\nu = \frac{1}{2}$.

is perturbed, e.g., by a Dirac-type pulse or a time-periodic forcing, the perturbation will grow further downstream (see Figs. 5 and 7). Although the Reynolds number in our study is higher than 10^{-7}, it is known that the flow pattern remains qualitatively the same (convective instabilities) but the growth rate depends on the viscoelastic behavior (which can be linked to a Weissenberg number) [39,40]. In fact, as the amplitude of the perturbations decreases with the decrease in the Reynolds number, it is necessary to introduce the constitutive equation of the studied polymer in order to get an accurate estimation of spatial growth rate. In a real coextrusion process, the growth in the perturbation amplitude further downstream should be avoided because it will not lead to a uniform interface height and may cause mixing of the fluid layers. Nevertheless, a partial and preliminary result based on the predictions in Sec. III can be made: the amplification of the perturbation amplitude further downstream could be reduced by decreasing the upper-layer thickness (polypropylene).

VI. CRITERION FOR SPATIALLY AMPLIFYING WAVES

For small temporal and spatial growth rates, the following approximate transformation relating these growth rates was proposed by Gaster [29] for α_x, the spatial amplification:

$$\alpha_x = -\sigma_r \left/ \left. \frac{\partial \sigma_i}{\partial \alpha} \right|_{\alpha = \alpha_\nu} \right. , \qquad (6.1)$$

where σ_r and α_ν are solutions of the dispersion relation (4.5):

$$D\left(\sigma_r - i2\pi\nu, \alpha_\nu\right) = 0. \qquad (6.2)$$

If the perturbation grows in amplitude with location x (spatially amplifying waves), α_x is positive; and if the perturbation amplitude decays with x, α_x shows a negative value. Gaster's relation is widely utilized for computing spatial growth rates using computed temporal growth rates. This reduces considerably the computation time because spatial stability computations are much more time consuming than

TABLE I. Amplification ratio, α_x, for $R_\mu = 0.1$ and Re $= 10$. α_ν is the wave number solution of dispersion relation (6.2), $\alpha_{x,G}$ is the amplification ratio calculated based on Gaster's formula (6.1), whereas $\alpha_{x,N}$ is the value obtained from the numerical results via Eq. (6.3).

	α_ν	$\alpha_{x,G}$	$\alpha_{x,N}$	α_ν	$\alpha_{x,G}$	$\alpha_{x,N}$
$\nu = \frac{1}{5}$	0.796	0.078	0.31	1.195	0.044	0.05
$\nu = \frac{1}{2}$	2.163	0.259	0.37	2.915	0.218	0.26

temporal stability ones. Moreover, Gaster's transformation allows us to obtain the spatial amplification in the entire domain of α. In [41], a mathematical example was presented in which all the premises of Gaster's analysis [29] were fulfilled. However, formula (6.1) gave incorrect results, indicating that the Gaster's transformation should be used with caution. In another study [42], on the other hand, it was found that relation (6.1) remains adequate for film flow down an inclined plane. Since for two-layer Poiseuille flow, the same kind of instability mechanism is expected (the liquid-air interface is replaced by a liquid-liquid interface) and the growth rates σ_r are rather small, it can be assumed that this relation would also work well in this case [35]. Reference [35] looks at coextrusion flow experimentally. It is shown in their Fig. 10 that the theoretical predictions based on Gaster's criterion are in quite good agreement with experimental data. In some ranges of wave number the two values do not agree well quantitatively but the source of discrepancy is well addressed in details in the same paper [35].

Gaster's criterion is now applied to the current linear stability formulation (Sec. IV), for a different set of parameters. The values of α_x for Re $= 10$ and $R_\mu = 0.1$ are listed in Table I. The influence of flow rate ratio and frequency is assessed by considering $R_Q = 2.3$ and 0.11, and $\nu = \frac{1}{5}$ and $\frac{1}{2}$. Note that the forcing frequency ν and wave speed σ_i, are related by $\nu = -\frac{\sigma_i}{2\pi}$. A crude spatial growth rate based on the numerical results can also be given by the formula

$$\alpha_x = \frac{\log\{\max_t[h(x_2,t) - h^s]\} - \log\{\max_t[h(x_1,t) - h^s]\}}{x_2 - x_1},$$

$$(6.3)$$

where x_1 and x_2 denote two different locations along the channel. The amplification ratios calculated based on estimate (6.3) and the simulations are also listed in Table I:

$$R_Q = 2.3, \quad R_Q = 0.11.$$

The positive values of α_x in Table I indicate that the perturbation will be amplified further downstream, which is in qualitative agreement with the numerical prediction (also see Fig. 7 for $R_\mu = 0.1$, $\nu = \frac{1}{2}$, Re $= 10$, and $R_Q = 2.3$). The agreement between the numerical amplification ratio, $\alpha_{x,N}$, and the amplification ratio based on Gaster's formula $\alpha_{x,G}$ is better for $\nu = \frac{1}{2}$ because the spatial periodicity of the perturbation of the Gaster's solution is smaller. In fact for $\nu = \frac{1}{5}$, it is necessary to perform direct numerical computations on a larger spatial range in order to get a disturbance with the spatial periodicity predicted by the dispersion relation. It is

worth noting that the code was run on a larger domain ($x_2 = 8$) and an amplification ratio of ~ 0.13 was obtained, which is much closer to Gaster's prediction, $\alpha_{x,G} = 0.078$. It is worth noting that the good agreement with Gaster's criterion (either quantitatively or qualitatively) is more of a hint in the right direction than a complete agreement. By looking at the Table I data, it can also be concluded that in the case of a less viscous upper layer, any increase in the upper-layer thickness will make the flow field more unstable. In return, the negative value of α_x in Table I means that the perturbation will be damped further downstream. Note the close quantitative agreement between the negative amplification ratio value based on Gaster's formula $\alpha_{x,G}$ and the numerical value $\alpha_{x,N}$ for $\nu = \frac{1}{2}$. In the case of the more viscous upper layer, any increase in the upper-layer thickness will result in a smaller value of α_x, finally stabilizing the flow. Although there is no difference between the signs of $\alpha_{x,G}$ and $\alpha_{x,N}$, one can see a very slight quantitative discrepancy between the two values, which is most likely due to the fact that Gaster's formula is based on the temporal *linear* stability results, whereas the numerical values are obtained from the *nonlinear* numerical solution on a finite domain in the x direction. Another interesting result can be extracted from Table I by considering the effect of forcing frequency. It can be seen that when the viscosity and flow rate ratios are such that the perturbation gets amplified further downstream, the decrease in the forcing frequency, ν, can destabilize the flow even more. On the other hand, the decrease in ν value has a stabilizing effect as the perturbation is damped downstream.

Valette *et al.* [39] studied the interface instability of the coextrusion flow of polyethylene and polystyrene both experimentally and theoretically (using the White-Metzner constitutive equation) in a slit geometry. For prototype industrial conditions, a stable (unstable) transition was found which bounds the occurrence of stable (unstable) sheets at the die exit. This transition is controlled by flow rate ratio and temperature (since the viscosities depend on the temperature). The dominant mode of instability was recognized to be of the convective type. Spatial amplification rates were then calculated for all studied conditions and showed that such an analysis is able to predict the occurrence of defects at the die exit. The spatial amplification rate of the perturbations was given in [39] as a function of forcing wave number for polyethylene and polystyrene solutions, a die gap of 2 mm, $T = 180\,^{\circ}\text{C}$, and $R_Q \sim 11.8$ ($Q_{PE} = 87.4$ g/min and $Q_{PS} = 7.4$ g/min). The corresponding R_μ value for these solutions is ~ 1.4. The current formulation predicts a negative value for

the spatial amplification factor α_x, whereas a positive value was observed both experimentally and theoretically for the White-Metzner model (see Fig. 10 in [39]). Given the high flow rate in this case, the current Newtonian fluid assumption may not be valid. The shear rate inside the system is very high, $\dot{\gamma} = O(10^3)\,\text{s}^{-1}$. In this case, viscoelastic and shear-thinning effects cannot be neglected.

VII. CONCLUSION

Two-layer thin-film flow inside a channel is examined in this study. The fluid density is assumed to be uniform over the flow domain, but the viscosity in each layer can be different. Interfacial tension has been neglected. The weighted residual approach first proposed by Amaouche *et al.* [31] is used for solving the problem, but additional simplifications are proposed to improve its legibility and appliance. The stability of two-layer Poiseuille flow is investigated for long wavelength limit and the formulas of the literature are recovered. The viscosity ratio R_μ seems to have a destabilizing effect on the flow with a thicker upper layer. When the upper layer is more viscous than the lower layer, the thickness ratio R_H seems to have a stabilizing effect on the flow.

In order to simulate the disturbance effect on a real coextrusion flow, the steady flow, which is simply the uniform flow of two layers of fluid inside a channel, was then perturbed in two different ways. First, by a Dirac-type pulse which is imposed on the lower-layer flow rate at $t = 0.5$, and second, by time-periodic forcing in the form of $q\,(x = 0, t) = [1 + 0.1\,\sin(2\pi\nu t)]\,q^s$ with ν being the forcing frequency. The perturbation takes the form of a wave packet which may or may not be amplified as it moves downstream depending on the values of the parameters involved in problem. In a real coextrusion process, the growth of the perturbation amplitude further downstream should be avoided because it will not lead to a uniform interface height and may cause mixing of the fluid layers. Finally, Gaster's criterion [29] was applied to the linear stability formulation for a different set of parameters to check if the perturbation grows in amplitude with location x, (spatially amplifying waves). The predictions based on Gaster's criterion were then compared with those obtained through the numerical solution of the reduced model showing close agreement.

APPENDIX A: COEFFICIENTS IN EQ. (3.17)

$$R_1 = (a_{17}h^7 + a_{16}h^6 + a_{15}h^5 + a_{14}h^4 + a_{13}h^3 + a_{12}h^2 + a_{11}h + a_{10})/D_1,$$
$$R_2 = (a_{29}h^9 + a_{28}h^8 + a_{27}h^7 + a_{26}h^6 + a_{25}h^5 + a_{24}h^4 + a_{23}h^3 + a_{22}h^2 + a_{21}h + a_{20})/D_2,$$
$$R_3 = (a_{35}h^5 + a_{34}h^4 + a_{33}h^3 + a_{32}h^2 + a_{31}h + a_{30})/D_3,$$
$$R_4 = (a_{47}h^7 + a_{46}h^6 + a_{45}h^5 + a_{44}h^4 + a_{43}h^3 + a_{42}h^2 + a_{41}h + a_{40})/D_4,$$
$$R_5 = (a_{57}h^7 + a_{56}h^6 + a_{55}h^5 + a_{54}h^4 + a_{53}h^3 + a_{52}h^2 + a_{51}h + a_{50})/D_5,$$

where

$$a_{17} = -2(R_\mu - 1)^3(1 + f),$$

$$a_{16} = (R_\mu - 1)^2(5R_\mu - 12)(1 + f) - 3(R_\mu^3 - 3R_\mu^2 + 3R_\mu - 1)q,$$

$$a_{15} = -4(R_\mu - 1)(R_\mu^2 - 6R_\mu + 7)(1 + f) + 6(R_\mu^3 - 4R_\mu^2 + 5R_\mu - 2)q,$$

$$a_{14} = -2(6R_\mu^2 - 21R_\mu + 16)(1 + f) - (2R_\mu^3 - 19R_\mu^2 + 34R_\mu - 17)q,$$

$$a_{13} = -2(7R_\mu - 9)(1 + f) - 4(2 - 3R_\mu + R_\mu^2)q,$$

$$a_{12} = (R_\mu - 4)(1 + f) + 3(R_\mu - 1)q,$$

$$a_{11} = -2(R_\mu - 2)q,$$

$$a_{10} = -q,$$

$$a_{29} = -4(R_\mu - 1)^3(9R_\mu - 10)(1 + f)^2 + 76(R_\mu - 1)^4(1 + f)q,$$

$$a_{28} = \left[-99\left(R_\mu^4 + 1\right) + 386R_\mu\left(R_\mu^2 + 1\right) - 594R_\mu^2\right]q^2 + (R_\mu - 1)^2\left(55R_\mu^2 - 238R_\mu + 192\right)(1 + f)^2$$
$$- 2(R_\mu - 1)^3(62R_\mu - 181)(1 + f)q,$$

$$a_{27} = \left(240R_\mu^4 - 1272R_\mu^3 + 2376R_\mu^2 - 1896R_\mu + 552\right)q^2 - 2(R_\mu - 1)\left(5R_\mu^3 - 112R_\mu^2 + 283R_\mu - 180\right)(1 + f)^2$$
$$+ 2\left(17R_\mu^2 - 230R_\mu + 337\right)(R_\mu - 1)^2(1 + f)q,$$

$$a_{26} = \left(-180R_\mu^4 + 1494R_\mu^3 - 3720R_\mu^2 + 3678R_\mu - 1272\right)q^2 + \left(-34R_\mu^3 + 312R_\mu^2 - 604R_\mu + 320\right)(1 + f)^2$$
$$+ \left(-4R_\mu^4 - 718R_\mu^2 + 106R_\mu^3 + 1218R_\mu - 602\right)(1 + f)q,$$

$$a_{25} = \left(48R_\mu^4 - 774R_\mu^3 + 2844R_\mu^2 - 3654R_\mu + 1536\right)q^2 + \left(-6R_\mu^2 + 136R_\mu - 120\right)(1 + f)^2$$
$$+ \left(-8R_\mu^3 + 126R_\mu^2 - 352R_\mu + 250\right)(1 + f)q,$$

$$a_{24} = \left(156R_\mu^3 - 1062R_\mu^2 + 1896R_\mu - 990\right)q^2 + \left(-11R_\mu^2 + 10R_\mu\right)(1 + f)^2 + \left(-56R_\mu^2 + 62R_\mu - 46\right)(1 + f)q,$$

$$a_{23} = \left(156R_\mu^2 - 420R_\mu + 264\right)q^2 - (2R_\mu - 8)(1 + f)^2 + 2q\left(11R_\mu^2 - 16R_\mu + 11\right)(1 + f),$$

$$a_{22} = (-18R_\mu + 48)q^2 + 2(3R_\mu - 7)(1 + f)q,$$

$$a_{21} = (18R_\mu - 48)q^2 + 2(1 + f)q,$$

$$a_{20} = 9q^2,$$

$$a_{35} = 3(R_\mu - 1)^2,$$

$$a_{34} = -4(R_\mu - 1)(R_\mu - 2),$$

$$a_{33} = 6(1 - R_\mu),$$

$$a_{32} = 0,$$

$$a_{31} = -1,$$

$$a_{30} = 0,$$

$$a_{47} = -262(R_\mu - 1)^3(1 + f),$$

$$a_{46} = (R_\mu - 1)^2(437R_\mu - 1100)(1 + f) - 297(R_\mu - 1)^3q,$$

$$a_{45} = -2(R_\mu - 1)\left(74R_\mu^2 - 721R_\mu + 893\right)(1 + f) - 54(R_\mu - 1)^2(10R_\mu - 23)q,$$

$$a_{44} = -\left(402R_\mu^2 - 1722R_\mu + 1384\right)(1 + f) - 27(R_\mu - 1)\left(8R_\mu^2 - 65R_\mu + 73\right)q,$$

$$a_{43} = (-378R_\mu + 506)(1 + f) + 108(R_\mu - 1)(5R_\mu - 13)q,$$

$$a_{42} = (33R_\mu - 76)(1 + f) + 351(R_\mu - 1)q,$$

$$a_{41} = 6(1 + f) - 54q,$$

$$a_{40} = 27q,$$

$$a_{57} = -7\text{Re}(R_\mu - 1)^2 f',$$

$$a_{56} = \text{Re}(R_\mu - 1)(16R_\mu - 27)f',$$

$$a_{55} = -20R_\mu(R_\mu - 1)^2(1 + f) - \text{Re}\left(9R_\mu^2 - 45R_\mu + 38\right)f' + 20\left(R_\mu^3 - 3R_\mu^2 + 3R_\mu + 1\right)q,$$

$$a_{54} = 20R_\mu(R_\mu - 1)(1 + f) - \text{Re}(17R_\mu - 22)f' + 100(R_\mu - 1)^2 q,$$
$$a_{53} = -20R_\mu(3R_\mu - 5)(1 + f) + \text{Re}(-R_\mu + 3)f' - 40\left(3R_\mu^2 - 8R_\mu + 5\right)q,$$
$$a_{52} = -60R_\mu(1 + f) - f'\text{Re} - 20\left(4R_\mu^2 + 14R_\mu - 10\right)q,$$
$$a_{51} = 100(R_\mu - 1)q,$$
$$a_{50} = 20q,$$

and

$$D_1 = \frac{5}{\text{Re}}(h - 1)^2[(R_\mu - 1)h^2 - 2(2R_\mu - 1)h - 1][(R_\mu - 1)h + 1]^2,$$
$$D_2 = \frac{140}{3\text{Re}}h(h - 1)^3[(R_\mu - 1)h^2 - 2(2R_\mu - 1)h - 1][(R_\mu - 1)h + 1]^3,$$
$$D_3 = \frac{5}{\text{Re}}(h - 1)[(R_\mu - 1)h + 1][(R_\mu - 1)h^2 + 2(1 - 2R_\mu)h - 1],$$
$$D_4 = 28D_1,$$
$$D_5 = 10(h - 1)^2[(R_\mu - 1)h + 1][(R_\mu - 1)h^2 + 2(1 - 2R_\mu)h - 1].$$

APPENDIX B: COMPARISONS WITH ASYMPTOTIC ANALYSIS OF THE NAVIER-STOKES EQUATION

Following notations in [22], new parameters are introduced: the layer thickness ratio $\varepsilon_p = R_H - 1$ and the viscosity ratio $m = R_\mu$. Then, the coefficients c_0 and c_1 of the relation (4.7) have the following forms:

$$c_0 = \frac{6\left(m + 2m\varepsilon_p + \varepsilon_p^2\right)\left(2\varepsilon + \varepsilon_p^2 + m\right)m\varepsilon(1 + \varepsilon_p)^2}{d_0^2},$$

$$c_1 = i\text{Re}\frac{3\left(m - \varepsilon_p^2\right)(m - 1)\varepsilon_p^2 f_1(\varepsilon_p, m)}{35d_0^5},$$

with

$$d_0 = m^2 + 2\varepsilon m\left(2\varepsilon_p^2 + 3\varepsilon_p + 2\right) + \varepsilon_p^4,$$
$$f_1 = (6\varepsilon_p + 1)m^7 + \left(-2\varepsilon_p - 9\varepsilon_p^2 - 120\varepsilon_p^3 - 88\varepsilon_p^4\right)m^6 + \left(32\varepsilon_p^2 + 344\varepsilon_p^3 + 821\varepsilon_p^4 + 1426\varepsilon_p^5 + 1096\varepsilon_p^6 + 224\varepsilon_p^7\right)m^5$$
$$+ \left(408\varepsilon_p^4 + 1642\varepsilon_p^5 + 3667\varepsilon_p^6 + 3424\varepsilon_p^7 + 1240\varepsilon_p^8 + 224\varepsilon_p^9\right)m^4$$
$$+ \left(224\varepsilon_p^5 + 1240\varepsilon_p^6 + 3424\varepsilon_p^7 + 3667\varepsilon_p^8 + 1642\varepsilon_p^9 + 408\varepsilon_p^{10}\right)m^3$$
$$+ \left(224\varepsilon_p^7 + 1096\varepsilon_p^8 + 1426\varepsilon_p^9 + 821\varepsilon_p^{10} + 344\varepsilon_p^{11} + 32\varepsilon_p^{12}\right)m^2 - \left(88\varepsilon_p^{10} + 120\varepsilon_p^{11} + 9\varepsilon_p^{12} + 2\varepsilon_p^{13}\right)m + 6\varepsilon_p^{13} + \varepsilon_p^{14}.$$

The relations given in Appendix A in [22] are recovered by changing the scaling for the velocity (the velocity at the interface instead of the mean velocity). That corresponds to dividing the above coefficients by the nondimensional velocity at the interface (twice for c_1):

$$u\left(y = \frac{1}{R_H}\right) = \frac{6m(1 + \varepsilon_p)^2\varepsilon_p}{m^2 + 4m\varepsilon_p + 6m\varepsilon_p^2 + 4m\varepsilon_p^3 + \varepsilon_p^4}.$$

[1] A. Oron, S. H. Davis, and S. G. Bankoff, Rev. Mod. Phys. **69**, 931 (1997).

[2] W. J. Schrenk and T. Alfrey Jr., in *Polymer Blends*, edited by D. R. Paul and S. Newman (Academic, New York, 1978), Vol. 2, p. 129.

[3] C. S. Yih, J. Fluid Mech. **27**, 337 (1967).

[4] Y. Renardy, Phys. Fluids **28**, 3441 (1985).

[5] T. I. Hesla, F. R. Pranckh, and L. Preziosi, Phys. Fluids **29**, 2808 (1986).

[6] S. G. Yiantsios and B. G. Higgins, Phys. Fluids. **31**, 3225 (1988).

[7] F. Charru and J. Fabre, Phys. Fluids **6**, 1223(1994).

[8] B. S. Tilley, S. H. Davis, and S. G. Bankoff, Phys. Fluids **6**, 3906 (1994).

[9] B. S. Tilley, S. H. Davis, and S. G. Bankoff, J. Fluid Mech. **277**, 55 (1994).

[10] M. E. Charles and L. U. Lilleleht, J. Fluid Mech. **22**, 217 (1965).

[11] T. W. Kao and C. Park, J. Fluid Mech. **52**, 401 (1972).

[12] D. Joseph, M. Renardy, and Y. Renardy, J. Fluid Mech. **141**, 309 (1984).

[13] A. P. Hooper and W. G. C. Boyd, J. Fluid Mech. **128**, 507 (1983).

[14] A. P. Hooper, Phys. Fluids **28**, 1613 (1985).

[15] A. P. Hooper and R. Grimshaw, Phys. Fluids **28**, 37 (1985).

[16] V. Shankar and V. Kumaran, J. Fluid Mech. **434**, 337 (2001).

[17] V. Shankar, J. Non-Newtonian Fluid Mech. **117**, 163 (2004).

[18] K. P. Chen, J. Non-Newtonian Fluid Mech. **40**, 155 (1991).

[19] D. Joseph and Y. Renardy, *Fundamentals of Two-fluid Dynamics, Part I: Mathematical Theory and Applications* (Springer-Verlag, New York, 1993).

[20] J. H. Southern and R. L. Ballman, J. Appl. Polym. Sci. **20**, 175 (1973).

[21] Y. Y. Su and B. Khomami, J. Rheol. **36**, 357 (1992).

[22] P. Laure, H. Le Meur, Y. Demay, J. C. Saut, and S. Scotto, J. Non-Newtonian Fluid Mech. **71**, 1 (1997).

[23] Y. Y. Su and B. Khomami, Rheol. Acta **31**, 413 (1992).

[24] J. L. White, R. C. Ufford, K. R. Dharod, and R. L. Price, J. Appl. Polym. Sci. **16**, 1313 (1972).

[25] T. C. Yu and C. D. Han, J. Appl. Polym. Sci. **17**, 1203 (1973).

[26] C. D. Han and Y. W. Kim, J. Appl. Polym. Sci. **20**, 2609 (1976).

[27] K. Alba, R. E. Khayat, and R. S. Pandher, Phys. Rev. E **77**, 056304 (2008).

[28] O. Takeshi, Phys. Fluids **11**, 3247 (1999).

[29] M. Gaster, J. Fluid Mech. **14**, 222 (1962).

[30] R. Quil and P. Manneville, Eur. Phys. J. B **15**, 357 (2000).

[31] M. Amaouche, N. Mehidi, and N. Amatousse, Phys. Fluids **19**, 084106 (2007).

[32] V. Y. Shkadov, Izv. Akad. Nauk SSSR, Mekh. Zhidk. Gaza **1**, 43 (1967).

[33] B. Vempati, A. Oztekin, and S. Neti, Acta Mech. **209**, 187 (2010).

[34] T. Cebeci and P. Bradshaw, *Momentum Transfer in Boundary Layers* (McGraw-Hill, New York, 1977).

[35] R. Valette, P. Laure, Y. Demay, and A. Fortin, Int. Polym. Process. **16**, 192 (2001).

[36] P. Huerre and A. Monkewitz, Annu. Rev. Fluid Mech. **22**, 473 (1990).

[37] P. Laure and A. Fortin [http://math.unice.fr/laure/articles/LF.pdf].

[38] G. M. Wilson and B. Khomami, J. Non-Newtonian Fluid Mech. **45**, 355 (1992).

[39] R. Valette, P. Laure, Y. Demay, and J.-F. Agassant, J. Non-Newtonian Fluid Mech. **121**, 41 (2004).

[40] H. K. Ganpule and B. Khomami, J. Non-Newtonian Fluid Mech. **81**, 27 (1999).

[41] L. Brevdo, Math. Mech. **72**, 305 (1992).

[42] L. Brevdo, P. Laure, F. Dias, and T. J. Bridges, J. Fluid Mech. **396**, 37 (1999).